

$K_L \rightarrow \pi^0 \nu \bar{\nu}$ at the AGS (E926) *

Akira Konaka[†]

TRIUMF

4004 Wesbrook Mall, Vancouver, B.C. V6T2A3 CANADA

Abstract

A proposed experiment to measure $K_L \rightarrow \pi^0 \nu \bar{\nu}$ at the AGS (E926) is described. It adopts a unique but general strategy of rare decay measurements with two independent rejection criteria, which allows reliable measurements of background levels. The method employs hermetic veto and full kinematic reconstruction using kaon time of flight and kinematic reconstruction of π^0 . Backgrounds are suppressed to a level well below an anticipated signal in the range $3 \pm 2 \times 10^{-11}$.

arXiv:hep-ex/9903016v1 11 Mar 1999

*talk presented at the “International Workshop on CP Violation in K”, 18-19 December 1998, KEK-Tanashi, Tokyo

[†]For the E926 collaboration (BNL, INR(Moscow), Kyoto, U.N.M., U.B.C., Jefferson Lab., TRIUMF, V.P.I., Yale), Email address: konaka@sitka.triumf.ca

1 Introduction

1.1 Physics Motivation

As discussed by the previous speakers, the rare decay $K_L \rightarrow \pi^0 \nu \bar{\nu}$ is unique among potential SM observables; it is dominated by direct CP violation [1] and is entirely governed by short-distance physics involving the top quark. As a consequence of unprecedented theoretical precision and anticipated experimental accessibility, a measurement of $K_L^0 \rightarrow \pi^0 \nu \bar{\nu}$ can unambiguously test the SM origin of CP violation and ultimately yield the most accurate determination of the CKM CP violating phase η . This rare decay mode therefore provides an exceptional and unique opportunity for making significant progress in our understanding of flavor-dynamics and CP violation. It is competitive with and complementary to future measurements in the B meson system. Absence of $K_L^0 \rightarrow \pi^0 \nu \bar{\nu}$ within the expected range of about $(3 \pm 2) \cdot 10^{-11}$ or a conflict with other CKM determinations would certainly indicate new physics.

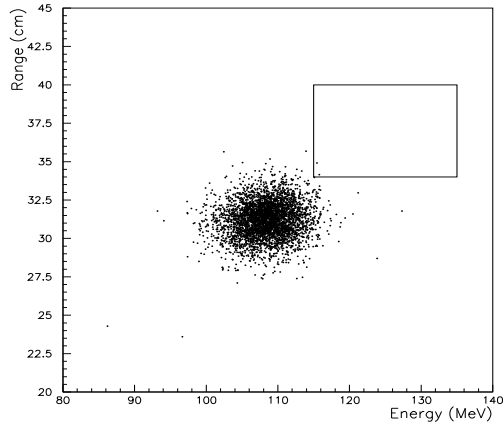
1.2 A strategy of the rare decay measurement

In this section, a unique but general strategy for rare decay measurements which was found to be essential in observing $K^+ \rightarrow \pi^+ \nu \bar{\nu}$ in E787, is described. The main challenge in such a very rare decay search is to control the systematic error in estimating the level of backgrounds. We have to make sure that there are no very rare software/hardware problems or unexpected rare background mechanisms that are not taken into account in estimating the background. In general, these potential problems are not well represented by Monte Carlo simulations, and one has to go back to the data to systematically study them. E787 analysis uses a tool called a “bifurcated analysis” along with a method to protect against bias due to small statistics. As will become clear, it is essential to have *two independent rejection criteria (or cuts)* for each background processes.

1.2.1 Bifurcated analysis

The bifurcated analysis of $K^+ \rightarrow \pi^+ \nu \bar{\nu}$ in the E787 experiment consists of two built-in independent selection criteria which are used to *measure* each background. Figure 1 shows $K^+ \rightarrow \pi^+ \pi^0$ background measurement as an example. In this example, the photon veto, which rejects $\pi^0 \rightarrow \gamma \gamma$ decays, and the charged particle kinematics (range, energy and momentum), which rejects the monochromatic π^+ , are taken as the two independent cuts. Because these two cuts address different particles in the final state, they are independent in principle. The scatter plot on the left in Figure 1 shows the energy versus range distribution when the photon veto cut is loosened. With this sample enhanced by a factor of 50, the rejection of the kinematic cut can be measured. The histogram on the right shows the momentum distributions before (the largest histogram) and after (the smallest histogram) the photon veto. The momentum peak is suppressed by a factor of 10^6 . It should be pointed out that the momentum line shape did not change after this

photon veto reversed
 $\times \sim 50$ enhancement



Selecting $K_{\pi 2}$ peak
 $\times \sim 100000$ enhancement

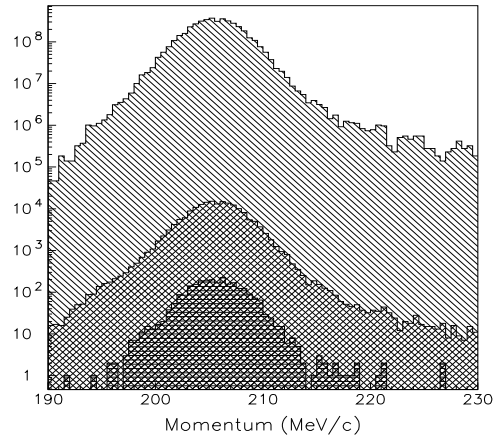


Figure 1: An example of a bifurcated analysis in the E787 $K^+ \rightarrow \pi^+\pi^0$ background analysis.

suppression, providing confidence that the two criteria are independent. All the kinematic variables used in the analysis are tested this way to see if there are any correlation with photon veto left.

The bifurcated analysis is a powerful way of measuring the background levels and their systematic uncertainties due to correlations. Because one can enhance the background by a large number, it also allows us to examine rare mechanisms and to develop detailed analysis cuts to reject them. Figure 2 shows time differences between the charged track

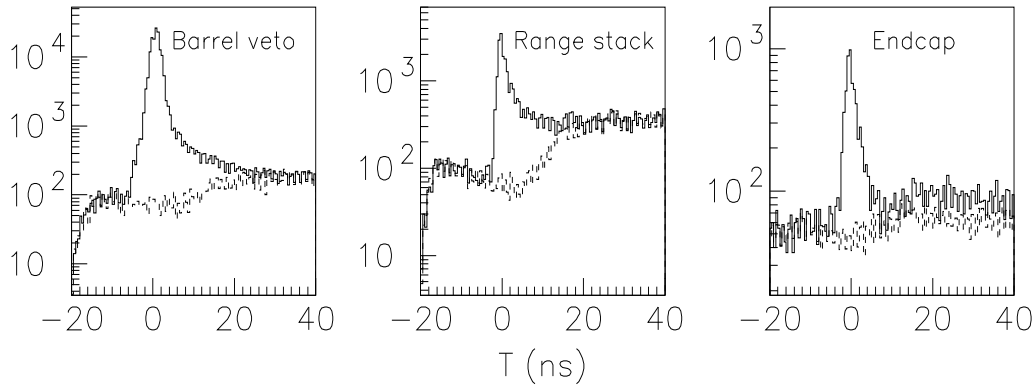


Figure 2: The time difference between the charged track and extra junk energies for the $K^+ \rightarrow \pi^+\pi^0$ kinematic peak events.

and extra energy for the $K^+ \rightarrow \pi^+\pi^0$ kinematic peak events in the 3 types of photon veto systems. The barrel veto is a lead/plastic scintillator sandwich, the range stack is a stack of plastic scintillators, and the endcap is made of pure CsI crystals. The solid lines show the data and the dashed lines show measured accidental rate from $K^+ \rightarrow \mu^+\nu$ events. For the barrel veto and range stack, there are non-Gaussian tails at larger times, which are understood as neutrons produced by photonuclear reactions (Figure 3). Neutrons from

photonuclear reactions leave late energy through n-p scattering in the plastic scintillation counters in the range stack and barrel veto. Using these data, photon veto cut positions in time versus energy space were optimized.

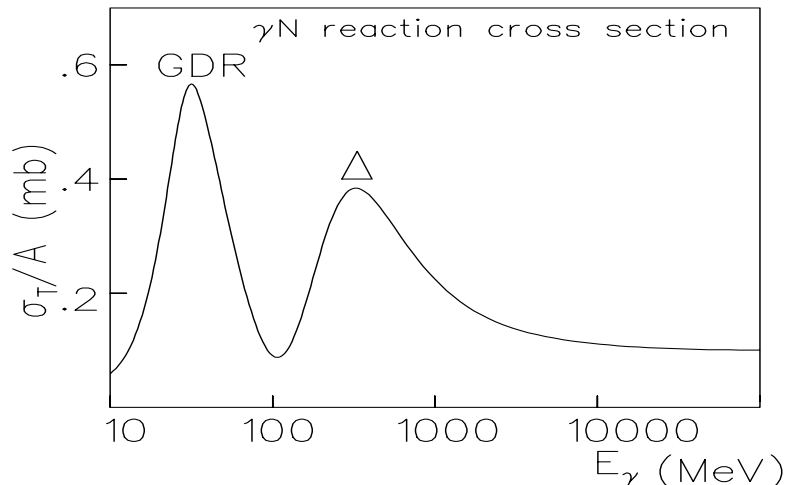


Figure 3: Photonuclear reaction cross section as a function of photon energy. The giant dipole resonance of nuclei is at around 20MeV, and the delta resonance of the nucleon is at around 300MeV. The cross section converges to an asymptotic value at high energy.

1.2.2 Protection against bias due to small statistics

From time to time, we see experimental evidence of a several standard deviation (σ) effect appear and then disappear as more statistics are accumulated. This can be understood considering only statistical effects, once we recognize the fact that one measurement out of a large number of experiments being performed should show such a large statistical fluctuation. The same thing would happen even in a single peak search experiment, such as Higgs search: Suppose we look for a peak in a distribution which spans a range 300 times larger than the width of the expected signal peak, we would expect on average one 3σ peak, whose probability is 0.27% ($300 \times 0.27\% \sim 1$). Confusion is caused when the number of trials, e.g. 300 of peak search regions, is not taken into account. This is often referred to as analysis bias.

The same bias shows up in rare decay analyses. Suppose we are left with one candidate event and found that one signal selection criterion, which is 99% efficient, removes it. We might conclude that the event is a background. However, if 100 such 99% efficient criteria are tried before finding the one criterion that removes the event, it is likely we would succeed in finding one even for a signal event ($100 \times 1\% = 1$). Again, what is important is to take the number of trials into account. In reality, we often look at an event display and various quantities to make a physics judgment on the event, in which procedure it is very difficult to quantify how many trials are performed. One way, which may be the only way, to protect against this analysis bias is to avoid such procedures in which one cannot quantify the number of trials.

There were three steps taken by the rare decay analysis, each of which required protection against potential bias:

- Candidate event selection (**Blind analysis**)
If we examine individual candidate events and develop selection cuts, we introduce analysis bias as discussed above. The way to avoid this is to develop cuts without examining the candidate events (“blind analysis”). The bifurcated analyses provide large data samples which are good representations of background. These samples allow us to develop analysis cuts without examining candidate events.
- Background measurement (**Training/Test samples**)
If there are no events left (upper limit only) at the end, the blind analysis might be sufficient. However, in order to observe the signal, one needs to avoid bias in the background measurement, to prove if the remaining events are signal or background. Again, when we examine each of the remaining background events, making many trials to find effective cuts and adopt only the ones that eliminate the remnant, we introduce a bias, namely we underestimate the background level. Because bifurcated analysis provides large background samples, we can afford to split them into two and use one for developing cuts (training sample) and the other for measuring the resulting background levels (test sample) to avoid the potential bias.
- Detailed examination of the candidates (**Signal/background likelihood**)
It is impossible to fully prove that there is nothing missed at all in the analysis at the end. In the case of bifurcated analysis, there may be a hidden correlation between two “independent” cuts which does not show up in the correlation tests as described in the previous section. We would eventually be forced to examine the candidate event to see if there is anything wrong with it. As discussed above, we could always find a distribution in which the candidate event is near the edge even

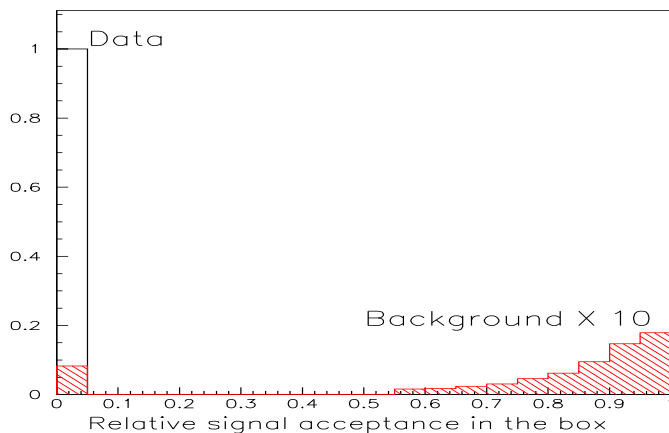


Figure 4: Signal likelihood function of E787 in the signal box. The shaded histogram shows the expected background distribution scaled up by a factor of 10. The candidate event is found to be in the cleanest region with a factor of 10 more rejection.

for the real signal event, if we look at enough quantities (enough trials). In order to examine the candidate event in an unbiased way, a signal likelihood function was prepared beforehand in the E787 analysis (Figure 4). The large background sample from bifurcated analysis provided enough statistics even inside the signal region. There was more confidence in the signal, because the event was in the cleanest region in the signal box with a factor of 10 more background rejection. It should be pointed out that this last step was feasible only because the experiment had extra background rejection capability (redundancy) beyond the final cut position.

2 Basic concept of the experiment

Figure 5 shows the π^0 energy distribution in the K_L center of mass frame ($E_{\pi^0}^*$) for the $K_L \rightarrow \pi^0 \nu \bar{\nu}$ and $K_L \rightarrow \pi^0 \pi^0$ ($K_{\pi_2}^0$) decays. The main background comes from the CP

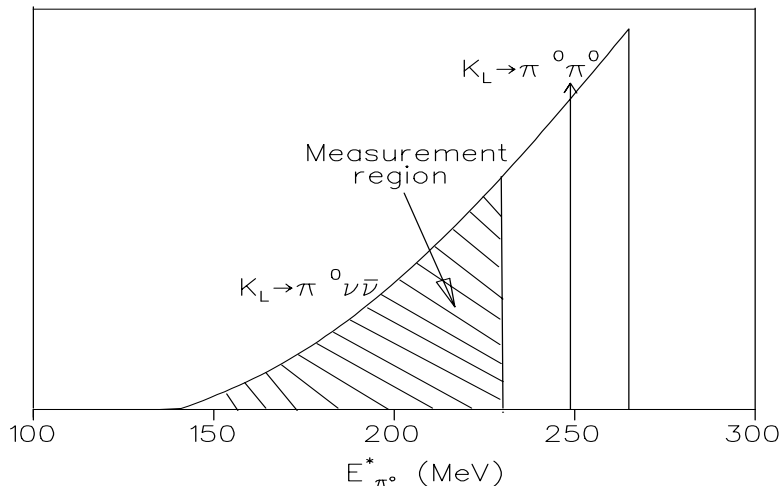


Figure 5: Energy spectrum of π^0 in the K_L center of mass frame.

violating decay $K_L \rightarrow \pi^0 \pi^0$ where 2 of the photons are missed. Even with the branching ratio of 9×10^{-4} and photon detection inefficiency of 10^{-4} per photon (the value that is achieved for higher energy photons in E787), the background appears at a single event sensitivity of $(9 \times 10^{-4}) \cdot (10^{-4})^2 \cdot 4 C_2 = 5.4 \times 10^{-11}$. This is larger than the central value of the Standard Model prediction of 3×10^{-11} . As we have seen in the previous section, it is very difficult to measure the background with only a photon veto cut. Thus, to increase the probability that the source of observed “ π^0 plus nothing” events is truly the $\pi^0 \nu \bar{\nu}$ mode another handle using *kinematics* is needed. By measuring the decaying K_L^0 momentum using time-of-flight, one can transform the π^0 momentum back to the K_L center of mass system on an event-by-event basis, and reject the monochromatic $K_{\pi_2}^0$ peak. With these two independent cuts of kinematics and photon veto, we can get sufficient background rejection and make a reliable measurement of the background.

Figure 6 shows a schematic view of the detector. A bunched K_L beam produced by the pulsed AGS proton beam decays in the decay region which is hermetically surrounded

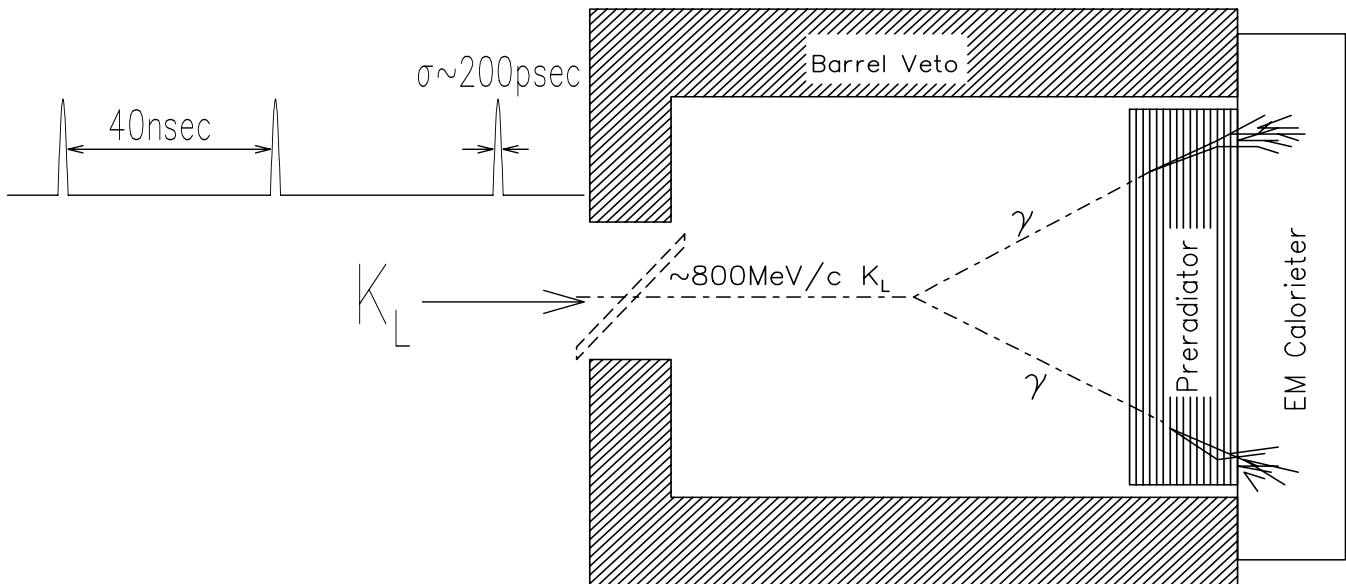


Figure 6: A schematic view of the detector.

by photon detectors. The directions of the photons are measured by a preradiator and the total energy is measured by an electromagnetic calorimeter. In the following sections, more detailed descriptions of the kinematic criteria and photon veto are given.

2.1 Full kinematic reconstruction and particle identification

Since the 3-body π^0 spectrum is the only observable in $K_L^0 \rightarrow \pi^0 \nu \bar{\nu}$, the most effective strategy for a clear measurement is to fully reconstruct the π^0 in the K_L center of mass frame. This can only be efficiently and unambiguously accomplished by completely measuring the kinematics of the decay photons including time, position, angle and energy and by determining the K_L momentum by time-of-flight from the production target. This method results in positive identification of the signal and effective suppression of the background since, for example, the two-body $K_{\pi_2}^0$ decay identifies itself by the unique momentum of the π^0 when viewed in the K_L rest frame. Once the K_L momentum is known, a large fraction of the $K_L^0 \rightarrow \pi^0 \nu \bar{\nu}$ phase space is available for detection and all the major sources of background become manageable.

Figure 7 shows the measured quantities in the experiment. The energies and times of the photons (E_γ, T_γ) are measured by the calorimeter and the directions are measured by the preradiator. The preradiator also accomplishes particle identification: The first layer of scintillator identifies whether it is a charged or neutral particle, and dE/dx and the track pattern discriminates photons from K_L and neutrons.

The K_L beam is collimated into a plane (slit beam). The decay vertex is measured by extrapolating the photon direction into the beam plane. The vertex can be obtained from one photon direction alone; the direction of the other photon, the time difference between the two photons, which corresponds to the path length difference between the two photons, and the π^0 mass work as extra constraints. These extra constraints are

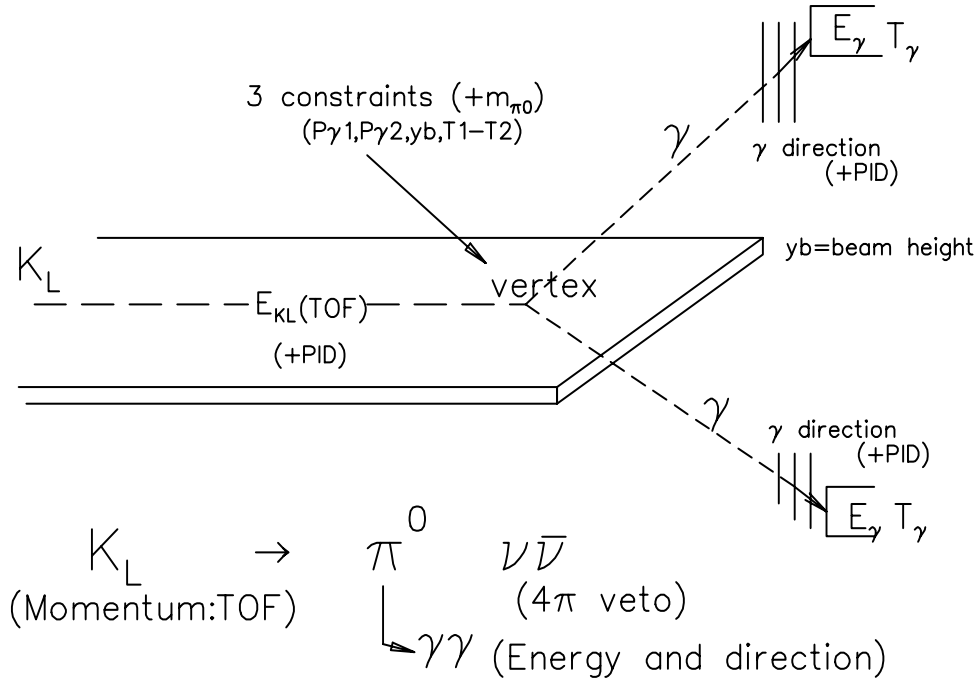


Figure 7: Quantities measured in the experiment.

effective in removing non-Gaussian tails, particularly in the angular measurements by the preradiator. The K_L energy is measured by time of flight using on RF bunched beam and direction is given by connecting the production target position and the decay vertex.

2.2 Photon veto

E787 has achieved a π^0 detection inefficiency of 10^{-6} at photon energies of 20–225 MeV using a lead/scintillator detector. The inefficiency for the lowest energy photons is $\sim 10^{-2}$ and appears to be mainly limited by sampling fluctuations. The inefficiency for higher energy photons is $\sim 10^{-4}$ and appears to be limited by sampling fluctuations, shower escape and photonuclear reactions which may be contributing at comparable levels. Although the E787 group has attempted to study the origin of the residual inefficiency through measurements and simulations, considerable uncertainty remains. Thus, assuring the achievement of substantially higher photon detection efficiencies, for instance, at higher photon energies than the existing measurements, may be extremely difficult to establish reliably without actually performing the relevant measurements. The uncertainties are even larger for the region below 20 MeV photon energy which will be preferentially populated by $K_{\pi^2}^0$ background events involving higher energy π^0 's than observed in E787. It is for these reasons that, although advancements in detection efficiency may be possible to achieve, we will only rely on small extrapolations from the E787 measurements in predicting the level of π^0 inefficiency.

The goal in the $K_L^0 \rightarrow \pi^0 \nu\bar{\nu}$ experiment is to have π^0 detection inefficiency approaching 10^{-8} . This is feasible since both photons are generally in the higher energy range of the

E787 measurements where single photon detection inefficiencies of 10^{-4} have been measured. Since we also have kinematic handles available, we can suppress those kinematic configurations of $K_{\pi 2}^0$ events with low energy missing photons and reasonably expect to achieve the goal.

Because the momentum of the K_L is tagged, we can obtain the energy of the missing photons in $K_{\pi 2}^0$ events by subtracting the measured energies of the two observed photons from the K_L energy. Requiring significant total missing energy (i.e. $(E(K_L) - E_{\gamma 1} - E_{\gamma 2})$) as is generally the case for $K_L^0 \rightarrow \pi^0 \nu \bar{\nu}$ events suppresses most potential background events that contain lower energy missing photons (where the inefficiency is greatest). However, in unusual cases when one of the missing photons has very high energy and one has very low energy an additional cut on missing mass (i.e. $\sqrt{(E(K_L) - E_{\gamma 1} - E_{\gamma 2})^2 - (\mathbf{P}(K_L) - \mathbf{P}_{\gamma 1} - \mathbf{P}_{\gamma 2})^2)}$) is effective. Because the missing mass in $K_{\pi 2}^0$ events is proportional to $\sqrt{E_{miss1} * E_{miss2}}$, where E_{miss} is the energy of a missing photon, the missing mass also becomes small for the asymmetric energy sharing case. Figure 8 shows the missing mass vs. missing energy distribution of photons for $K_{\pi 2}^0$ and $K_L^0 \rightarrow \pi^0 \nu \bar{\nu}$ events. After removing the low missing mass and low missing energy region, we can suppress the low energy photons to achieve 10^{-8} detection inefficiency for the two missing photons in $K_{\pi 2}^0$ events.

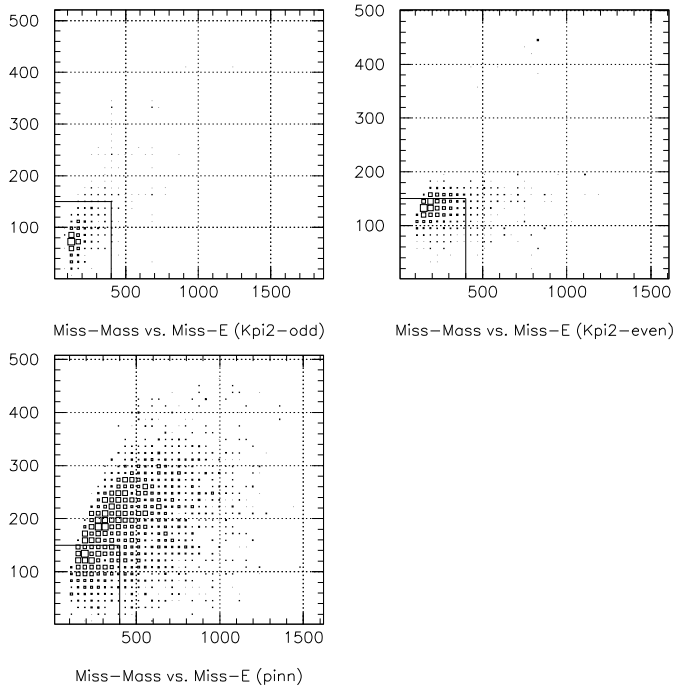


Figure 8: Missing mass vs. missing energy distribution of photons for $K_{\pi 2}^0$ odd, $K_{\pi 2}^0$ even and $K_L^0 \rightarrow \pi^0 \nu \bar{\nu}$ events.

The effect of small missing mass can be seen more directly by comparing $E_{\pi 0}^*$ distributions before and after the photon veto cut for $K_{\pi 2}^0$ odd background events where one

photon from each π^0 is missed (Figure 9). A dramatic peak above the $E_{\pi^0}^*=230\text{MeV}$ after photon veto cut directly corresponds to the small missing mass¹. This is one of the main reasons why the phase space below $K_{\pi^2}^0$ peak ($E_{\pi^0}^*=249\text{MeV}$) is used for the signal search region.

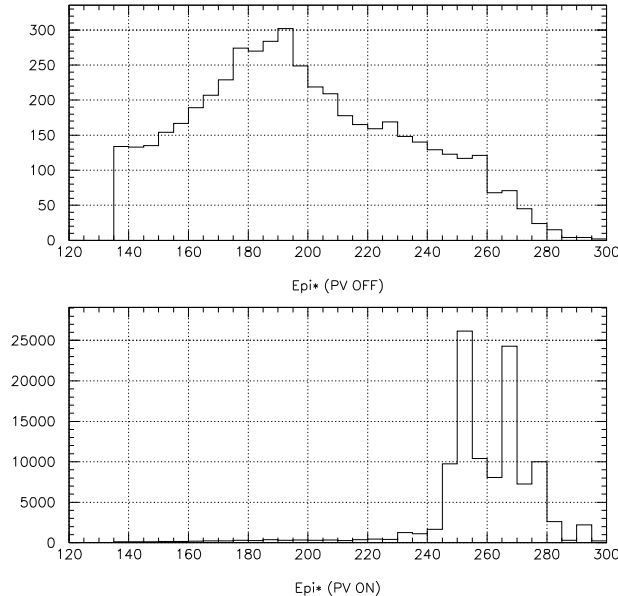


Figure 9: π^0 energy distribution in the K_L center of mass system ($E_{\pi^0}^*$) for $K_{\pi^2}^0$ odd events before (top) and after (bottom) photon veto cuts. The vertical scale of the bottom figure is in the unit of 10^{-8} events.

3 Experimental design

3.1 An overview

Figure 10 shows a layout of the proposed experiment. A $500 \mu\text{sr}$ solid angle neutral beam is extracted at 45° to produce a “soft” K_L spectrum peaked at $0.65 \text{ GeV}/c$. Kaons in the range from about $0.5 \text{ GeV}/c$ to $1.3 \text{ GeV}/c$ will be used. The vertical acceptance of the beam (0.004 r) is kept much smaller than the horizontal acceptance (0.125 r) so that effective collimation can be used to severely limit beam halos. Downstream of the final beam collimator is a 3.5 m long decay region which is surrounded by the main detector. Approximately 16% of the kaons decay yielding a decay rate of about 25 MHz . The beam region is evacuated to a level of 10^{-7} Torr to suppress neutron induced π^0 production. The decay region is surrounded by an efficient Pb/scintillator photon veto detector. A

¹There is a one-to-one correspondence between $E_{\pi^0}^*$ and missing mass: $E_{\pi^0}^* = \frac{m_K^2 + m_{\pi^0}^2 - m_{miss}^2}{2m_K}$. For small missing mass, $E_{\pi^0}^*$ is large.

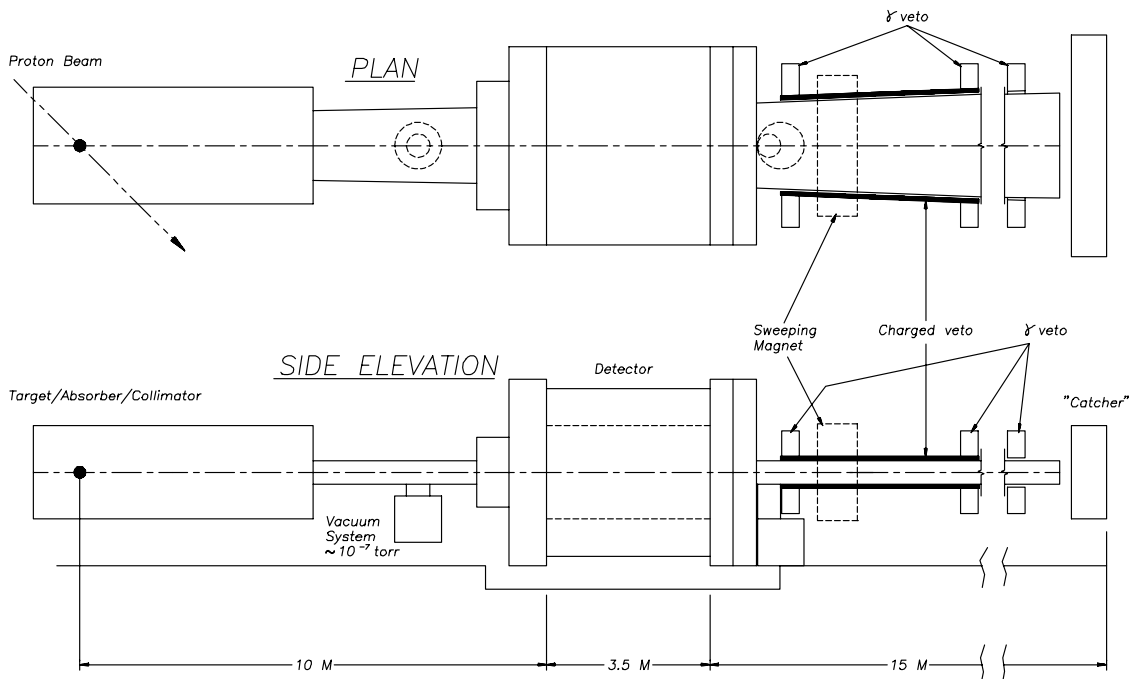


Figure 10: Layout of the $K_L^0 \rightarrow \pi^0 \nu \bar{\nu}$ experiment.

Čerenkov detector (“catcher”) covers the beam hole at the end of the beam line, 15 m downstream of the detector.

3.2 The K_L beam

In recent years the AGS has achieved new records of intensity for synchrotrons. The present SEB peak extraction current is 7×10^{13} protons/pulse. Coupled with a high current micro-bunched beam, good duty factor and extended availability during the RHIC era,² the AGS is the ideal accelerator site for rare neutral kaon decay experiments employing time-of-flight. The spectrum of neutral kaons produced at 45 degrees shown in Figure 11 (left) was obtained using a code based on a fit to CERN charged particle production data[3]. The spectrum shape is consistent with large angle charged kaon production data (BNL-E802) fitted by semi-phenomenological analytical methods[4][5]. The K_L production yield is consistent within a factor of 2 between these two estimations.

Neutrons from the production target could limit the beam intensity to be tolerated. In particular, neutrons above the pion production threshold can cause accidental backgrounds. The neutron momentum spectrum for 45° is shown in Figure 11 (right). At this large production angle, the neutron flux is largely suppressed above 800MeV/c, the pion production threshold of the n-p interaction.

The micro-structure of the beam provides further suppression of the neutrons. Fig-

² RHIC is projected to operate for 30 to 40 weeks per year and requires injection from the AGS for 2 hours/day. Thus, approximately 22 hours/day are available for AGS proton operation.

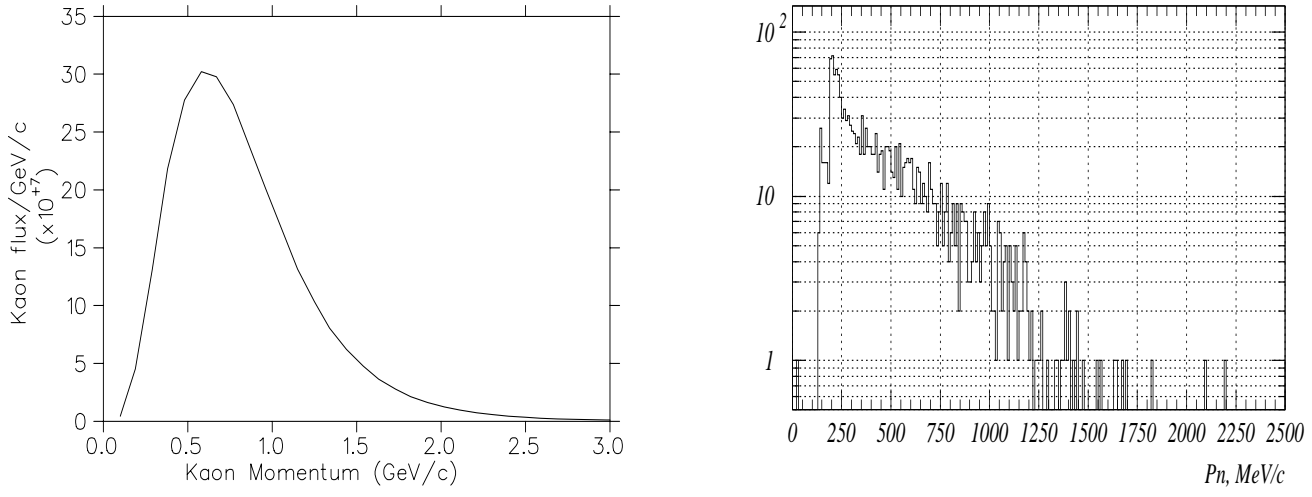


Figure 11: Momentum distribution of K_L and neutron fluxes

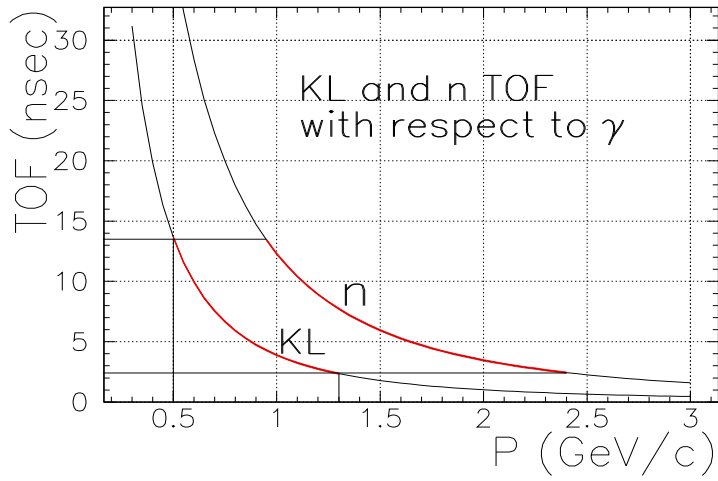


Figure 12: Arrival time of K_L 's and neutrons with respect to photons at 10m downstream from the production target.

ure 12 shows the arrival time of K_L s and neutrons with respect to photons at 10m from the production target. Neutrons with momenta between 0.9 and 2.4 GeV/c fall into our arrival time of interest (i.e. K_L with momenta between 0.5 and 1.3 GeV/c). Within this time window, the neutron to K_L ratio is improved by a factor of 5. Despite the fact that a low energy beam is used here, the effective n/K_L ratio is as good as or better than in higher energy experiments.

3.3 The detector

In the forward detection region the primary photon detector system illustrated in Figure 13 consists of two sections: a fine grained preradiator in which the photons are

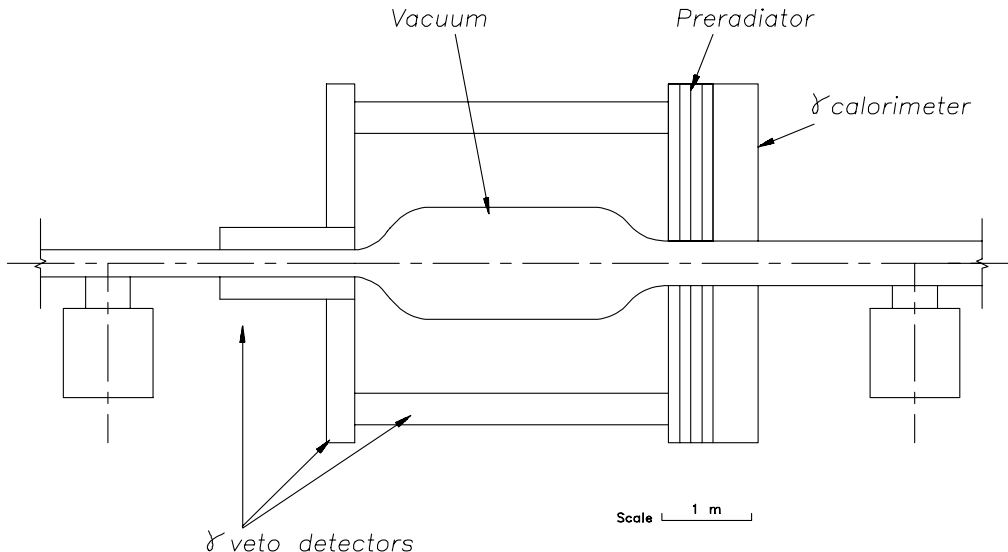


Figure 13: $K_L^0 \rightarrow \pi^0 \nu \bar{\nu}$ detector.

converted and the first e^+/e^- pair is tracked, followed by an 18 radiation length (X_0) calorimeter in which the remaining energy of the photon shower is measured. The preradiator consists of 42 layers each with plastic scintillator, $0.03 X_0$ of heavy metal and dual coordinate drift chambers. The preradiator which has a total effective thickness of $1.5 X_0$ functions to measure the photon positions and directions accurately in order to allow reconstruction of the K_L decay vertex while also contributing to the achievement of sufficient energy resolution. The calorimeter is constructed using thin Pb sheets formed to accept scintillating fibers in an arrangement similar to that recently made for the KLOE experiment at DAΦNE; in our implementation of the calorimeter, a significantly higher visible light fraction will be used to further improve the energy resolution. In order to reduce the cost of the detector, we are also considering a shashlik calorimeter, which is made of layers of thin Pb sheet and plastic scintillator read out by WLS fibers running perpendicular to the layers.

The barrel photon detector is made of layers of 1mm lead and 7mm extruded scintillator. The light from the scintillator is read out by embedded wave length shifter (WLS)

fibers. A prototype test with 4-m long WLS fibers shows a light yield of 12.1 p.e./MeV with a timing resolution of $\sigma = 0.85 \text{ nsec}$ [6]. Downstream of the main π^0 detector, a beam hole photon counter consists of layers of lead and lucite or aerogel Čerenkov detectors designed to be insensitive to neutrons. An initial prototype test using tagged photon and neutron beams shows promising results satisfying the experimental requirements [7].

4 Expected background levels and sensitivity

The dominant background for $K_L^0 \rightarrow \pi^0 \nu \bar{\nu}$ is the CP violating decay $K_L \rightarrow \pi^0 \pi^0$ ($K_{\pi 2}$) with a branching ratio of 9×10^{-4} . By tagging the K_L momentum as well as determining the energy and direction of γ s, one can reconstruct the kinematics. In the case of even pairing where one π^0 is missing, a kinematic cut on the monochromatic $E_{\pi^0}^*$ is effective. In the case of odd pairing where one photon from each π^0 is missed, the π^0 mass requirement ($m_{\gamma\gamma}$) is effective. An additional photon energy cut $E_{\pi^0}^*$ vs. $|E_{\gamma 1}^* - E_{\gamma 2}^*|$, where $E_{\gamma 1}^*$ and $E_{\gamma 2}^*$ are the energies of γ s in the K_L center of mass system, is also very effective in further suppressing the $K_{\pi 2}^0$ background.

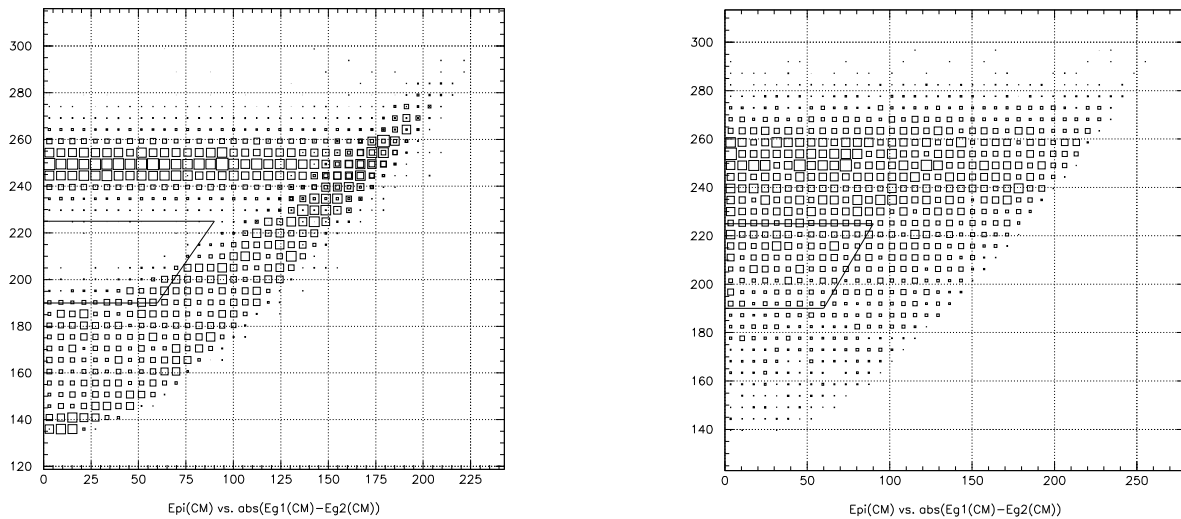


Figure 14: Distributions of $E_{\pi^0}^*$ vs. $|E_{\gamma 1}^* - E_{\gamma 2}^*|$ after π^0 mass requirement for the $K_L \rightarrow \pi^0 \pi^0$ (left) and for the signal (right). The solid line encloses the signal region.

Figure 14 shows distributions of $E_{\pi^0}^*$ vs. $|E_{\gamma 1}^* - E_{\gamma 2}^*|$, after π^0 mass requirement for the $K_L \rightarrow \pi^0 \pi^0$ (left) and for the signal (right). The band at $E_{\pi^0}^* = 249 \text{ MeV}$ corresponds to the even pairing background, which is suppressed by a $E_{\pi^0}^*$ cut at $225 \text{ MeV}/c$ as discussed above. The remaining band corresponds to the odd pairing background, which is confined into the band due to the constraint of 2 detected photons to form the π^0 mass. The solid line shows the signal region. As can be seen in the plots, we can obtain further background suppression at the cost of a modest acceptance loss. This redundancy in background rejection provides a safety margin in the experiment as well as a tool to positively identify

the signal. Table 1 gives the estimated acceptance factors for the $K_{\pi 2}^0$ backgrounds.

Requirement	$\pi^0\nu\bar{\nu}$	$\pi^0\pi^0$ odd	$\pi^0\pi^0$ even
γ combinations	1	4	2
solid angle	0.36	0.34	0.37
$m_{\gamma\gamma} = m_{\pi}$	0.72	0.08	0.74
E_{π}^*	0.38	0.76	0.008
photon veto		1.3×10^{-8}	4.2×10^{-8}
Photon energy cuts	0.35	0.07	0.17
BR		9×10^{-4}	9×10^{-4}
γ conv. and reconst.	0.45	0.45	0.45
Acceptance	0.016	3.5×10^{-14}	1.6×10^{-14}

Table 1: Acceptance for $K_{\pi 2}^0$ backgrounds.

Other potential sources of background include neutron production of π^0 s, other K_L decays like K_{e3} and $K_L \rightarrow \gamma\gamma$ and $\Lambda \rightarrow n\pi^0$ decays. Suppression of most backgrounds is accomplished by the hermetic high efficiency photon detector along with kinematic constraints. A summary of the background estimates is given in Table 2. The signal is estimated to exceed the background by an order of magnitude with the backgrounds dominated by $K_{\pi 2}^0$. We expect that the actual background levels will be determined reliably from the data.

Process	Modes studied	Main	events
$K_L \rightarrow \pi^0\nu\bar{\nu}$			70
K_L decays ($\bar{\gamma}$)	$\pi^0\pi^0, \pi^0\pi^0\pi^0, \pi^0\gamma\gamma$	$\pi^0\pi^0$	7
$K_L \rightarrow \gamma\gamma$	$\gamma\gamma$	$\gamma\gamma$	0.04
K_L decays (\overline{chrg})	$\pi^{\pm}e^{\mp}\nu, \pi^{\pm}\mu^{\mp}\nu, \pi^+\pi^-$	$\pi^-e^+\nu$	0.01
K_L decays ($\bar{\gamma}, chrg$)	$\pi^+\pi^-\pi^0, \pi^{\pm}l^{\mp}\nu\gamma, \pi^{\pm}l^{\mp}\nu\pi^0, \pi^+\pi^-\gamma$	$\pi^+\pi^-\pi^0$	0.003
Other decays	$\Lambda \rightarrow \pi^0n, K^- \rightarrow \pi^-\pi^0, \Sigma^+ \rightarrow \pi^0p$	$\Lambda \rightarrow \pi^0n$	0.03
Interactions	n, K_L, γ	$n \rightarrow \pi^0$	0.5
Accidentals	n, K_L, γ	n, K_L, γ	0.3

Table 2: Estimated event levels for signal and background.

Table 1 gives factors leading to the estimated acceptance of approximately 1.6%. It includes the solid angle, photon conversion and reconstruction factors and phase space ($E_{\pi 0}^*$) acceptance in addition to the photon energy cuts discussed above. The inefficiency due to accidental spoiling of good events is estimated to be $< 10\%$ for a threshold of a few MeV and a timing window of 2 ns. The expected number of $K_L^0 \rightarrow \pi^0\nu\bar{\nu}$ events to be accumulated for 8000 hours of beam is ~ 50 assuming the SM central value for the branching ratio of $B = 3 \times 10^{-11}$.

5 Summary and prospects

A detector system has been presented to measure the rare decay $K_L^0 \rightarrow \pi^0 \nu \bar{\nu}$. The experiment is designed to allow definitive observation of a large sample of events with a signal that exceeds backgrounds by an order of magnitude. Special features of the AGS allow provision of an intense pulsed beam of neutral kaons suitable for time-of-flight measurements. The two independent signal selection criteria of photon veto and kinematics allow large background rejection and reliable measurement of the background levels. Significant redundancies and contingency factors are built into the technique. The standard model origin of CP violation will be confirmed and the complex phase parameter η determined to a precision of $\leq 15\%$ or the absence of $K_L^0 \rightarrow \pi^0 \nu \bar{\nu}$ can be established at a level inconsistent with the standard model.

References

- [1] L. Littenberg, Phys. Rev. **D39** (1989) 3322.
- [2] A.J. Malensek, *Empirical formula for thick target particle production*, FNAL Preprint FN-341, October 1981.
- [3] H.W. Atherton *et al.*, CERN Report CERN 80-07, 1980.
- [4] T. Abbott *et al.*, Nucl. Instrum. Methods **A290** (1990) 41, T. Abbott *et al.*, Phys. Rev. **D45** (1992) 3906.
- [5] P. Kapinos, E926 technical note #005.
- [6] Y. Kudenko and O. Mineev, E926 technical note #008.
- [7] T. Nomura *et al.*, E926 technical note #013.